

Evaluation of the Town Energy Balance (TEB) Scheme with Direct Measurements from Dry Districts in Two Cities

V. MASSON

Centre National de Recherches Météorologiques, Toulouse, France

C. S. B. GRIMMOND

Atmospheric Science Program, Department of Geography, Indiana University, Bloomington, Indiana

T. R. OKE

Department of Geography, University of British Columbia, Vancouver, British Columbia, Canada

(Manuscript received 31 October 2001, in final form 9 May 2002)

ABSTRACT

The Town Energy Balance (TEB) model of Masson simulates turbulent fluxes for urban areas. It is forced with atmospheric data and radiation recorded above roof level and incorporates detailed representations of the urban surface (canyon geometry) to simulate energy balances for walls, roads, and roofs. Here the authors evaluate TEB using directly measured surface temperatures and local-scale energy balance and radiation fluxes for two "simple" urban sites: a downtown area within the historic core of Mexico City, Mexico (stone buildings five to six stories in height), and a light industrial site in Vancouver, British Columbia, Canada (flat-roofed, single-story warehouses). At both sites, vegetation cover is less than 5%, which permits direct evaluation of TEB in the absence of a coupled vegetation scheme. Following small modifications to TEB, notably to the aerodynamic resistance formulations, the model is shown to perform well overall. In Mexico City, with deep urban canyons and stone walls, almost two-thirds of the net radiation is partitioned into storage heat flux during the day, and this maintains large heat releases and an upward turbulent sensible heat flux at night. TEB simulates all of these features well. At both sites TEB correctly simulates the net radiation, surface temperatures, and the partitioning between the turbulent and storage heat fluxes. The composite wall temperature simulated by TEB is close to the average of the four measured wall temperatures. A sensitivity analysis of model parameters shows TEB is fairly robust; for the conditions considered here, TEB is most sensitive to roof characteristics and incoming solar radiation.

1. Introduction

Although a general understanding of the interactions between the atmosphere and urbanized areas based on carefully conducted experimental studies is emerging (see, e.g., Rotach 1995; Grimmond and Oke 1999a), the complexity and diversity of cities around the world often means observational studies are limited, either to a particular site or a single physical process. Numerical models have been developed to simulate the urban climate, but to date most of these models have been formulated either at the microscale (building and/or urban canyon) (e.g., Mills 1997; Arnfield and Grimmond 1998; Arnfield et al. 1998), or at the mesoscale (whole city), using vegetation-atmosphere transfer models originally developed for other surface types, but with parameters modified for application to the urban environment (e.g.,

Best 1998; Taha 1999). In an attempt to couple the two scales, Masson (2000) developed the Town Energy Balance (TEB) scheme, which can be used on its own for densely urbanized areas or with the Interactions between Soil, Biosphere, and Atmosphere (ISBA) model (Noilhan and Planton 1989) when vegetation is also present. TEB incorporates canyon geometry, with three typical surfaces—roof, wall, and road—in order to reproduce the effects produced by buildings. A specific energy balance is computed for each of these three surfaces. This approach is relatively simple, but it still allows most of the physical effects associated with the urban energy balance to be reproduced, including radiative trapping (longwave and shortwave), the momentum flux, the turbulent sensible and latent heat fluxes, heat storage uptake and release, and water and snow interception. The anthropogenic heat fluxes due to traffic and industry are prescribed, and they are implicitly computed for domestic heating by the use of a minimum internal building temperature.

Masson (2000) validated the radiative portions of

Corresponding author address: Dr. Valéry Masson, Centre National de Recherches Météorologiques, 42 av Coriolis, 31057 Toulouse Cedex, France.
E-mail: valery.masson@meteo.fr

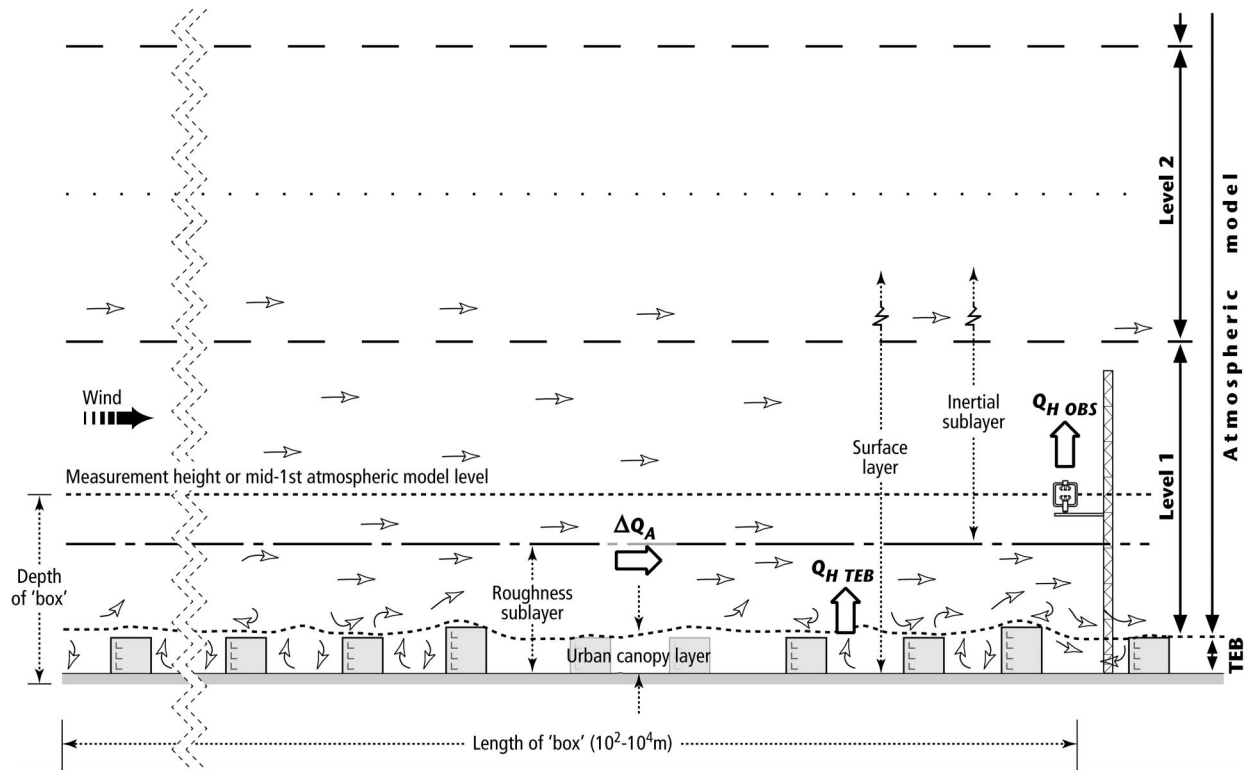


FIG. 1. Coupling of TEB within an atmospheric model with relation to measured and modeled variables. Dashed lines are the limits of the atmospheric grid boxes. Dotted lines are the middle of each grid box. For definition of the box see text. Here ΔQ_A is the advection flux below the measurement height.

TEB; however, only sensitivity experiments were conducted for the complete scheme. Here the objective is to present an independent evaluation of TEB using directly measured surface temperatures and surface energy balance fluxes for two “simple” urban sites. One is a portion of the historic core of Mexico City, Mexico, the other is a light industrial site in Vancouver, British Columbia, Canada. At both sites vegetation cover is less than 5% of the plan area (Grimmond and Oke 2002, their Fig. 5) but the sites are otherwise very different in terms of the structure and building construction. These tests allow direct evaluation of TEB and the appropriateness of the assigned parameter values and their sensitivity/robustness. Evaluation of the combined TEB–ISBA scheme, relevant to vegetated urban areas, is being pursued separately. TEB has been incorporated into MesoNH, the French community mesoscale model (Lafore et al. 1998), but here we consider the offline or stand-alone version.

2. The urban energy balance

Fundamental to this paper is the concept of the urban surface energy balance, defined by (Oke 1988)

$$Q^* + Q_F = Q_H + Q_E + \Delta Q_S + \Delta Q_A \quad [\text{W m}^{-2}], \quad (1)$$

with Q^* being the net all-wave radiation, Q_F the an-

thropogenic heat flux, Q_H the turbulent sensible heat flux, Q_E the turbulent latent heat flux, ΔQ_S the storage heat flux, and ΔQ_A the net advective heat flux. In numerical models, such as TEB, each of the surface energy balance fluxes in (1) can be addressed independently. In this study, because the sites chosen have very little vegetation cover and there was no precipitation or irrigation, Q_E is set to zero. The TEB–ISBA scheme, when operated in the offline mode, does not explicitly resolve the ΔQ_A term in (1). The model is forced with a temperature (T_a), humidity (q_a), and wind speed (U_a) measured in the inertial sublayer (Fig. 1). For TEB online, these are at the middle of the first atmospheric level, and for TEB offline they are at the measurement height. The rooftop level is the surface of the atmospheric model, so the TEB computed sensible heat flux (Q_{HTEB}) for the urban canopy is assigned at the base of the first atmospheric grid box (Figs. 1 and 2).

The modeled output fluxes (Q_H , Q_E , outgoing long-wave radiation $L\uparrow$ and outgoing shortwave radiation $K\uparrow$, when coupled to a 3D flow model, are assigned as input at the surface of the atmospheric model (the base of level 1 in Fig. 1), while forcing variables correspond to the midpoint of the level 1 grid. Note that the surface of the atmospheric model is located at the top of the mean topography and the building (roughness element) height for the individual grid square. In the 3D case,

the fluxes are then used to calculate the values of T_a , q_a , and U_a at the next time step. These interact with the surrounding grids, so the ΔQ_A term can be resolved. The impact on the surface fluxes is returned by the forcing (T_a , q_a , and U_a) driving the next time step of the TEB–ISBA surface scheme. If ΔQ_A is positive (usually because of energy supplied by the surface), this energy comes from the Q_H term convected from the surfaces, so Q_H at a higher level (typically the middle of level 1) is smaller by an amount ΔQ_A . The converse holds for a negative advection flux (Q_H increasing with height). In this manner the vertical profile of Q_H is affected by this advection flux.

When the energy balance is measured, however, (1) must be modified to read

$$Q^* = Q_H + Q_E + \Delta Q_S \text{ [W m}^{-2}\text{]}. \quad (2)$$

The terms in (2) are evaluated here by measurements at the top of a “box,” following the concept of Oke (1987, 1988) illustrated in Fig. 1. The height of the box extends from above the roughness sublayer to a depth in the ground where there is no vertical flux over the period of concern. The height of the box is typically about two times the height of the buildings. The horizontal dimension of the box is sufficient to ensure that microscale inhomogeneity merges into a representative local-scale property. The height and length of the box must be sufficient to ensure that microscale variability of fluxes in the source area (or “footprint”) is eliminated by turbulent mixing in the roughness sublayer, but not so great that the source area extends upwind into anomalous land cover. Thus, Q_{HOBS} is located in the inertial layer, at a height sufficient to avoid microscale effects found in the roughness sublayer, but not so high that anomalous upwind surfaces are sampled.

The ΔQ_A and Q_F do not appear explicitly in (2). If the land cover in the source area of the sensors is approximately homogeneous at the local scale, ΔQ_A is minimized and can be neglected. This can also be achieved at less than completely homogeneous sites through filtering the data by wind direction to eliminate sectors with anomalous surface cover. Heat released by combustion of fuels (Q_F) is a net source of energy in cities; however, the instruments used to measure Q^* , Q_H , and Q_E sense such anthropogenic contributions. Hence the total measured fluxes include this term, although the exact partitioning is not known. Adding an additional Q_F term to (2) would therefore double-count this source.

Here three components (Q^* , Q_H , and Q_E) are measured directly and ΔQ_S is determined as the residual of (2). In effect this means that storage changes in the volume of the box are expressed as an equivalent flux density through the top surface of the box. This has the effect that the net measurement errors incurred in estimating the other terms, including ΔQ_A , accumulate in ΔQ_S . It should be noted that closure of measured energy balances is rarely achieved, either over simple sites

where micrometeorological theory is most likely to hold (e.g., Foken and Oncley 1995) or more complex sites such as forests (e.g., Lee 1998). This contributes to flux uncertainty, especially of ΔQ_S , when resolved as a residual.

Given the differences between the modeled and measured energy balances [i.e., (1) and (2)], exact correspondence between measured and modeled fluxes is not to be expected. In particular, comparisons of the turbulent fluxes are affected by the assumption of zero evaporation by TEB (because ISBA is not run). This means TEB should overestimate Q_H by the value of measured Q_E . Here, Q_H calculated by TEB is compared at the measurement height with the sum of measured $Q_H + Q_E$. As discussed above, offline TEB Q_H values at this height include ΔQ_A . Thus from a modeling perspective the grid cell is regarded as homogeneous, but from the measurement perspective the area is homogeneous only if the site has sufficiently extensive fetch to minimize local-scale ΔQ_A (Fig. 1). Therefore, in the evaluation of the model in the offline version, it is necessary to assume that the turbulent fluxes Q_H and Q_E from top of the urban canopy layer (where TEB fluxes are computed; Fig. 1) to the top of the box (where the measurements are made) remain the same.

3. Observations

Here we present a brief overview of the observation methods used to gather data appropriate to the evaluation of TEB; more complete details are available in Grimmond and Oke (1999b), Oke et al. (1999), and Voogt and Grimmond (2000).

a. The study sites

Data were collected for Mexico City (referred to here as Me93) for a 7-day period during the dry season in December 1993 (Oke et al. 1999). The study site is located in the historic core of the city (see Fig. 1 of Oke et al. 1999) where the buildings are mainly institutional and commercial. In the vicinity of the measurement location, the mean building height is 18.4 ± 6.6 m. The average complete-to-plan area ratio (or the three-dimensional aspect ratio; Voogt and Oke 1997), λ_c , is 1.75. Average (3D) surface cover for the dominant source areas for the flux measurements is 25% impervious, 32% roofs, and 42% walls (Oke et al. 1999). Vegetation is negligible ($\sim 1\%$). In the street canyons and alleys adjacent to the tower, the sky view factor varies from about 0.22 to 0.51. Based on an inventory of materials within the radius of 500 m around the Me93 tower site, walls are made of concrete (two thirds) or stone (one third), with roofs of concrete, tar, sheet metal, or tile. Building walls and roofs are usually grey or brown. The roads are paved with concrete or asphalt, or surfaced with tiles, cobblestones, or flagstones.

Data were also collected for 15 days, in August 1992,

at a light industrial site in Vancouver, British Columbia (hereinafter referred to as V192), during an extended period of drought. The area is characterized by flat-roofed buildings one to three stories in height (average height 6.9 ± 2.5 m, λ_c is 1.39), used for light industry and as warehouses. The buildings are arranged in city blocks, with east–west and north–south orientation (see Fig. 3 of Voogt and Oke 1997). The axis of the main blocks and alleys run east–west between the main streets. Less than 5% of the plan area is covered by vegetation. Most buildings are made of concrete, and roads and pathways are made of asphalt and concrete.

b. Measured surface energy balance fluxes and forcing data

At each site, instruments were mounted high enough above the surface to ensure that the measurement box (Fig. 1) is representative of the integrated *local scale* (horizontal length scales of $\sim 10^2$ – 10^4 m). In Mexico City and Vancouver, equipment was mounted at 28.4 and 28.5 m above ground, respectively. In both cases the turbulent fluxes were measured using eddy covariance techniques and radiometry was used to determine Q^* . At the V192 site, ground heat flux plates were installed at a depth of 80 mm with temperature sensors above to account for flux divergence between the soil surface and the heat flux plates. In addition, standard meteorological data, needed as input for TEB, were collected at both sites.

The primary meteorological variable that forces TEB, incoming solar radiation ($K\downarrow$), was not measured at either site. However, $K\downarrow$ data were collected by the Institute of Geophysics, Universidad Nacional Autónoma de México at the university (~ 13 km south of the Me93 site), and by the Canadian Atmospheric Environment Service at the Vancouver International Airport (~ 8 km south of V192 site). Using previous studies on the spatial variation of $K\downarrow$, and patterns of air pollution and flow in the two cities, we assessed the degree to which the measured solar forcing might differ from that at the validation site. We conclude this may amount to a few percent too low (typically less than 5%) in the afternoon at Me93, but it is likely to be negligible (less than 1%) at V192. Incoming longwave radiation ($L\downarrow$) was not measured at either site but was calculated using observed air temperature and humidity following the method of Prata (1996).

In Mexico City, the surface temperatures of a roof and two roads in canyons adjacent to the site were measured by infrared thermometers. In Vancouver, the surface temperatures of four walls (one facing each cardinal direction), the roof, and the inside of the east-facing wall of a building at the site were measured using similar instruments. These observations do not provide a representative sample of all facets found within the local-scale turbulent source area (typically 15 – 40×10^3 m² by day, larger at night) at either site. Rather, they rep-

resent fairly typical microscale surfaces to provide some guidance as to the thermal conditions of small areas (sensor field of view about 5 – 10 m²).

In addition, airborne infrared measurements were conducted at the Vancouver site during one day at three different times: morning, mid-, and late afternoon. These measurements give the surface temperatures of each type of facet (walls, roofs, sunlit and shaded roads) at the local scale, an area more comparable with that of the source area of the turbulent fluxes. Therefore, even though only one day of data is available, it is of great interest to the validation of TEB. Note that the airborne measured wall temperatures compare well with the wall measurements made from a vehicle (Voogt and Oke 1997).

4. Implementation of TEB

Small modifications were made to the scheme originally presented in Masson (2000), notably to the aerodynamic resistance formulations (those indicated with thick lines in Fig. 2).

- The road resistance here follows a roughness length formulation, instead of that of Rowley et al. (1930), although the latter is still used for walls. This modification is included because of analyses of the V192 site, where roads are important and where airborne measured road temperatures allow discrimination between the two formulations (see section 5b). The road roughness length is set to 50 mm. This is much larger than the commonly used roughness for asphalt (<1 mm). However, 50 mm is considered to be a reasonable value when obstacles of the order of 1 m are present, as is the case for roads with cars, pedestrians, signs, lamp posts, bollards, etc. Sample calculations using a morphometric formula (Grimmond and Oke 1999a) show the roughness length can even be larger than the values used here if numerous cars and trucks are present.
- The temperatures of internal roof and wall layers are now linked to the internal temperature of the buildings (T_{ibld}) using a standard resistance (R_i) equal to 0.123 K m W⁻¹, based on building insulation values (McMullan 1992). In Masson (2000), T_{ibld} was directly applied to the inner surfaces, whereas here R_i mimics both the convection and the radiative interactions in the building. This modification has negligible effect, except for poorly insulated buildings, such as warehouses with metal roofs. In such cases the temperatures of the wall and roof inner layers now have greater diurnal amplitude, leading to larger amplitude for the outside surfaces.
- A new temperature evolution equation is used to represent the annual cycle of the internal temperature inside the buildings (especially for warm temperatures in summer):

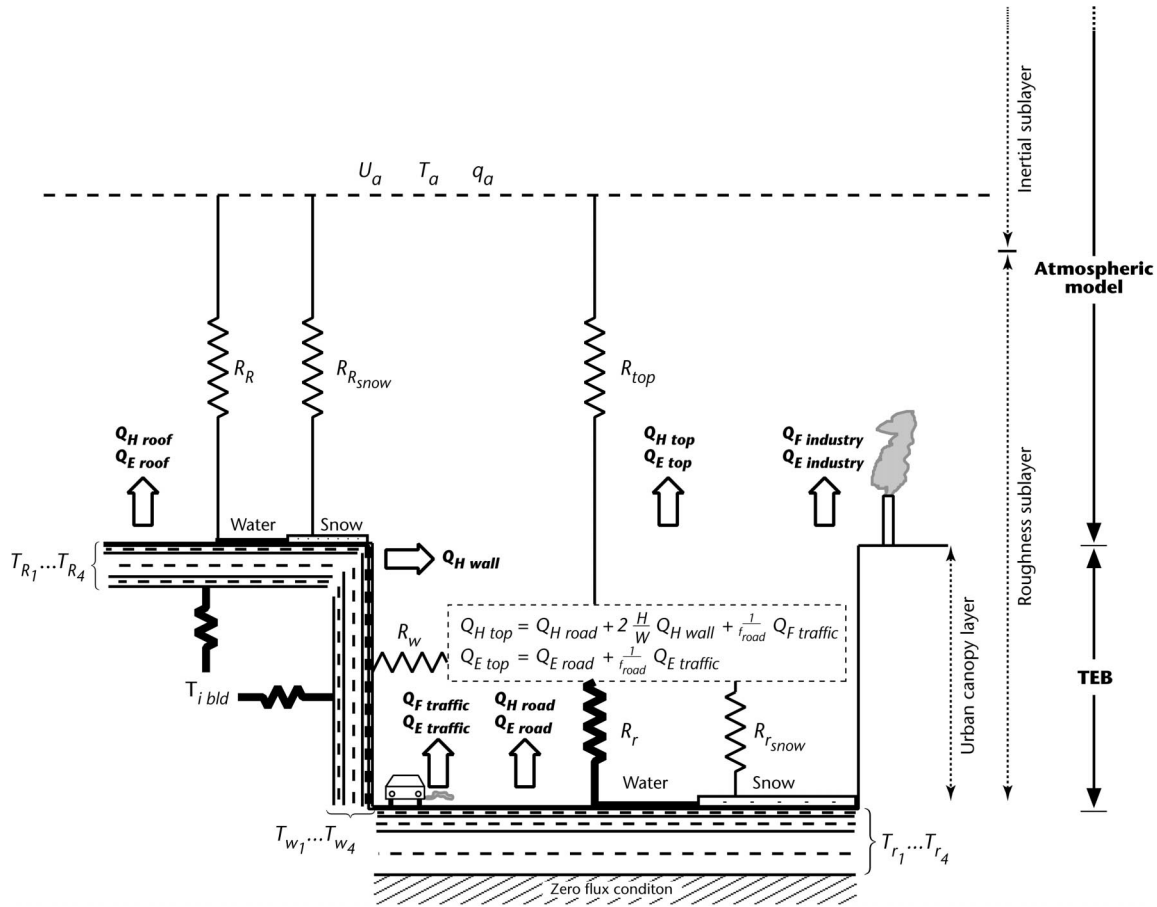


FIG. 2. Schematic representation of the surfaces (roof, wall, road indicated by subscript R , w , and r , respectively), prognostic temperatures (T), and aerodynamic resistances (R) used in TEB and the output fluxes. Resistances shown with thick lines have been altered from the original scheme (Masson 2000). Thus, $Q_{HTEB} = f_{roof} Q_{Hroof} + f_{road} Q_{Htop} + Q_{Findustry}$ and $Q_{ETEB} = f_{roof} Q_{Eroof} + f_{road} Q_{Etop} + Q_{Eindustry}$.

$$T_{ibld}^+ = T_{ibld}^- \left(\frac{\tau - \Delta\tau}{\tau} \right) + T^* \left(\frac{\Delta\tau}{\tau} \right),$$

where T_{ibld}^+ and T_{ibld}^- are the temperatures at the future and previous time step, respectively, Δt is the time step, τ is equal to 1 day, and T^* is the average of the internal (ceiling, wall, and floor) surface temperatures. However, as in the initial version of the scheme, T_{ibld}^+ has a minimum value, in order to represent anthropogenic heating.

The scheme is initialized with the meteorological data. No anthropogenic heat flux is prescribed. The parameters listed in Tables 1 and 2 are used to initialize the scheme in Me93 and V192. In both cases the morphometric parameters are weighted according to the wind direction frequency to be as consistent as possible with the observed fluxes. The roof, wall, and road fractions are calculated from Grimmond and Oke (1999b). The road is estimated to be composed of concrete (40%) and asphalt (60%) pavement (50 mm thick), over stone aggregate (0.2 m) and gravel and sandy clay soil. In general, the thermal parameters and emissivities are esti-

mated from data listed in the American Society of Heating, Refrigerating, and Air-Conditioning Engineers handbook (ASHRAE 1989). The albedo values are based on those listed for roofs, walls, and roads (Oke 1987).

At V192 the building walls are made of uninsulated concrete. The warehouse, where the microscale surface temperatures were observed, had a roof with a steel layer overlaid by a thin gravel layer. However, as most of the other warehouse roofs within this vicinity are made of concrete, topped with a thin insulation layer and gravel, this configuration is used in TEB (Table 2).

5. Evaluation of TEB

a. Mexico City

1) SURFACE TEMPERATURES AT THE MICROSCALE

Since TEB computes only one road surface temperature, independent of direction, the TEB value is compared to the average of two road surface temperature measurements (one in an S–N, one in an E–W street). The general form of the diurnal evolution of roof and

TABLE 1. Input parameters for the TEB scheme for the Vancouver light industrial (VI92) and Mexico City historic core (Me93) sites.

Parameters	Unit	Mexico City	Vancouver
Geometric parameters ^a			
Building fraction ^b	—	0.55	0.51
Building height ^b	m	18.8	5.8
Wall/plane area ratio ^b λ_c	—	0.75	0.39
Canyon aspect ratio ^b : H/W	—	1.18	0.39
Roughness length ^b	m	2.2	0.35
Radiative parameters ^c			
Roof albedo	—	0.20	0.12
Wall albedo	—	0.25	0.50
Road albedo	—	0.08	0.08
Roof emissivity	—	0.90	0.92
Wall emissivity	—	0.85	0.90
Road emissivity	—	0.95	0.95
Thermal parameters ^c (see Table 2 for values)			
Roof		Asphalt roll on concrete, good insulation	Thin gravel over concrete, poor insulation
Wall		Massive, thick, stone or concrete, insulation, 25% window	Concrete without insulation
Road		Asphalt 60%, concrete 40% on gravel, sandy clay	Asphalt 60%, concrete 40% on gravel, sandy clay
Roof roughness length	m	0.15	0.15
Road roughness length	m	0.05	0.05
Temperature initialization			
Inside building temperature	°C	20	23
Deep soil temperature	°C	22	20

^a Local-scale parameters.

^b Source: Grimmond and Oke (1999a).

^c Microscale parameters of individual facets.

road temperatures are correctly reproduced by TEB (Fig. 3, Table 3). However, TEB roof temperatures show larger diurnal amplitudes than those of the instrumented roof, with faster warming and cooling rates. This may be due to larger storage in the roof by TEB or to incorrect specification of the roof materials (see section

6 for a sensitivity test). A way to correct the daytime overestimation might be to increase the roughness length of the roof and hence the removal of heat via Q_H . It must also be appreciated that the observations are only for one roof. The TEB road temperature has both the correct temporal course and diurnal amplitude,

TABLE 2. Thermal parameters for roofs, walls, and roads used in TEB for the Vancouver and Mexico City sites. Layer sequence: 1 is nearest to the surface. Here d is thickness of layer (m), C is heat capacity of layer ($\text{MJ m}^{-3} \text{K}^{-1}$), and λ is thermal conductivity ($\text{W m}^{-1} \text{K}^{-1}$).

	Mexico City				Vancouver			
	1	2	3	4	1	2	3	4
Roof layer	Asphalt roll	Concrete (stone)	Insulation	Gypsum	Gravel	Gravel	Insulation	Concrete
d	0.01	0.1	0.05	0.025	0.01	0.02	0.01	0.030
C	1.7	1.5	0.25	0.87	1.76	1.76	0.04	2.21
λ	0.2	0.93	0.03	0.16	1.4	1.4	0.03	1.51
Wall layer	Stone/window	Stone/window	Stone/window	Insulation/window	Dense concrete	Dense concrete	Concrete	Dense concrete
d	0.015	0.12	0.30	0.015	0.010	0.02	0.14	0.03
C	1.54	1.54	1.54	0.32	2.11	2.11	1.00	2.11
λ	0.88	0.88	0.88	0.21	1.51	1.51	0.67	1.51
Road layer	Asphalt/concrete	Asphalt/concrete	Stone aggregate	Gravel and soil	Asphalt/concrete	Asphalt/concrete	Stone aggregate	Gravel and soil
d	0.01	0.04	0.20	1.00	0.01	0.04	0.20	1.00
C	1.74	1.74	2.00	1.40	1.74	1.74	2.00	1.40
λ	0.82	0.82	2.1	0.4	0.82	0.82	2.1	0.4

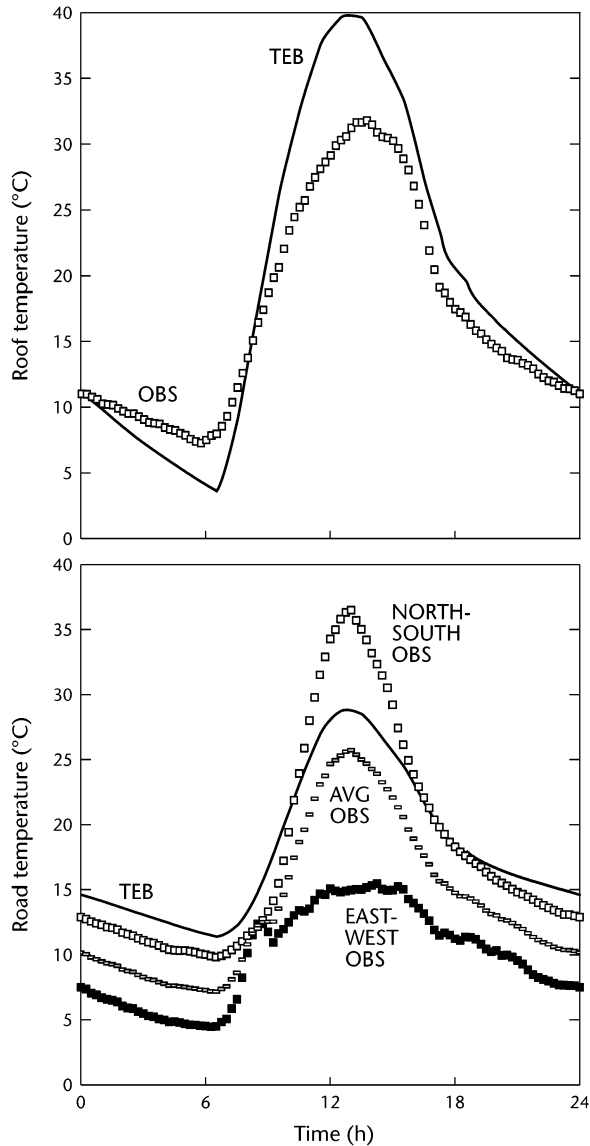


FIG. 3. Ensemble mean diurnal cycle for 6 days of measured and modeled surface temperatures for the Mexico City site: (top) roof surface temperature, and (bottom) road surface temperature.

but there is a bias of about +4 K. Given the uncertainties in using a calculated $L\downarrow$ (especially at night), the large difference between the observed temperatures in the two canyons (25 K during the day), and the microscale (rather than local scale) representativeness of the measurements, this is considered a good result.

2) ENERGY FLUXES AT THE LOCAL SCALE

TEB is evaluated using the measured hourly energy fluxes: net radiation, sensible heat flux, and storage heat flux (Fig. 4 gives the ensemble mean results and Table 4 the summary statistics).

During the night, the observed Q^* mean is -103 W m^{-2}

TABLE 3. Performance statistics for surface temperatures in Mexico City and a Vancouver light industrial site. Bias = TEB - obs.

	Bias (K)	Rmse (K)
Mexico City		
Average road temperature	+4	4.2
Roof temperature	+1.9	4.5
Vancouver		
YD 223–236 (all)		
Wall temperature	+2.3	3.0
Roof temperature	+2.5	7.4
YD 225–231 (period 1)		
Wall temperature	+1.9	2.4
Roof temperature	+1.7	7.5
YD 232–236 (period 2)		
Wall temperature	+2.7	3.7
Roof temperature	+3.6	7.2

m^{-2} , while TEB is only -82 W m^{-2} . The daytime Q^* is well reproduced (Table 4). The observed daytime $\Delta Q_s/Q^*$ ratio is very high (0.58); hence uptake of sensible heat into storage is more efficient than its convection to the boundary layer over this densely built-up district. This can probably be attributed to the thermal properties of the construction materials, the large 3D surface area exposed by this area of dense building and deep canyons, and the relatively light winds during the observation period (the mid- to late afternoon maximum speeds were $<3.5 \text{ m s}^{-1}$). TEB reproduces this result well; the simulated $\Delta Q_s/Q^*$ ratio is 0.56 (Table 4). The observations show little hysteresis in the diurnal relation between the ΔQ_s and the Q^* , and again TEB reproduces this well (Fig. 5). Similarly, TEB produces ΔQ_s fluxes of the correct magnitude, especially for the daytime maximum.

The nocturnal measurements show the heat release from the urban fabric to be larger than the Q^* drain (nighttime $\Delta Q_s/Q^* = 1.21$). This imbalance maintains an average upward-directed Q_H of 21 W m^{-2} . The model produces a nighttime $\Delta Q_s/Q^*$ ratio of 1.17, but since the calculated Q^* intensity is smaller than observed, the release of stored heat is also underestimated by 30 W m^{-2} . Therefore, the modeled Q_H reaches only 12 W m^{-2} , on average. However, it is encouraging that TEB is able to create a positive Q_H every night, including the cloudy night, as observed (not shown).

The observed rapid increase of Q_H (reaching between 50 and 100 W m^{-2}) in the early morning is not simulated by the model. The observed increase in Q_H might correspond to energy released from traffic (Q_f) during the morning commuter activity that is not included in these TEB runs. Ichinose et al. (1999), for example, report a traffic-induced heat flux in downtown Tokyo reaching 60 W m^{-2} .

Thus in summary, TEB is able to reproduce correctly most of the behavior of the fluxes typical of the Me93 central city site, including the relatively low Q^* in the

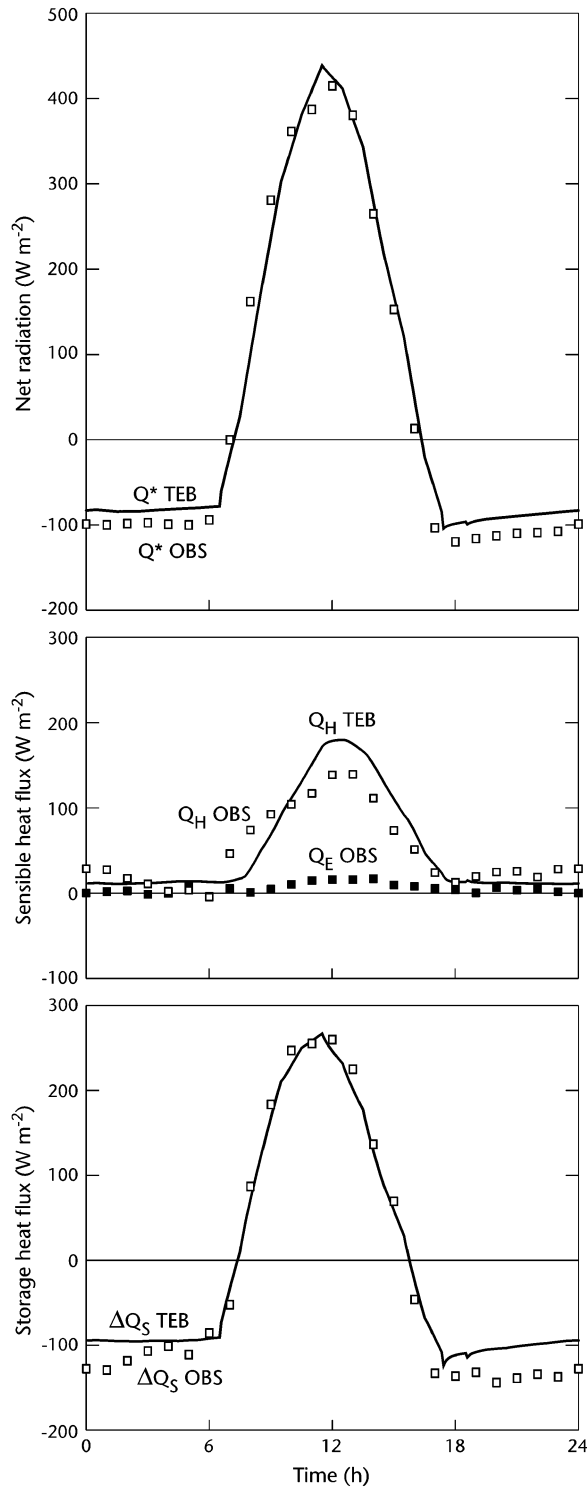


FIG. 4. Ensemble mean diurnal cycle of measured and modeled surface energy balance fluxes for 6 days at the Mexico City site: (top) net all-wave radiation, (middle) total turbulent flux, and (bottom) storage sensible heat flux.

TABLE 4. Performance statistics of TEB for heat fluxes ($W m^{-2}$) at the Mexico City site. Average [observed (obs), modeled (TEB)], bias (TEB - obs), and rmse.

	Heat flux	Q^*	$Q_H + Q_E$	ΔQ_S
Overall period	Obs	45	57	-12
	TEB	55	54	1
	Bias	10	-3	13
	Rmse	32	25	39
Daytime	Obs	257	108	149
	TEB	252	113	139
	Bias	-5	5	-10
	Rmse	41	32	45
Nighttime	Obs	-103	21	-125
	TEB	-82	12	-95
	Bias	21	-9	30
	Rmse	24	18	35

winter, the large daytime heat uptake by the urban fabric, and the positive Q_H at night.

b. Vancouver light industrial site

1) SURFACE TEMPERATURES AT THE MICRO- AND LOCAL SCALES

The surface temperature observations include in situ observations of individual roof, wall, and road facets of a warehouse, that is, at the microscale; and airborne measurements at 1000, 1400, and 1700 LST on one day [yearday (YD) 228] of a large number of buildings and canyons, that is, at the local scale. The latter is most appropriate to use in the evaluation of TEB. For the rest of the observations our discussion focuses on two periods: period 1, six sunny days (YD 225–231) characterized by a sea breeze in the early afternoon; and period 2, five more cloudy days (YD 232–236) when the sea breeze is much weaker and occurs only in the late afternoon.

The observed microscale *roof* temperatures show a very strong diurnal cycle, with variations of 50 K (Fig.

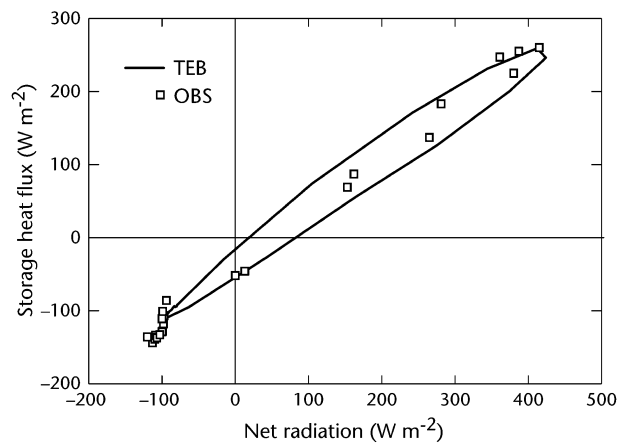


FIG. 5. Ensemble mean (6 days) measured and modeled (TEB) hysteresis loop relating the storage heat flux to the net radiation at the Mexico City site.

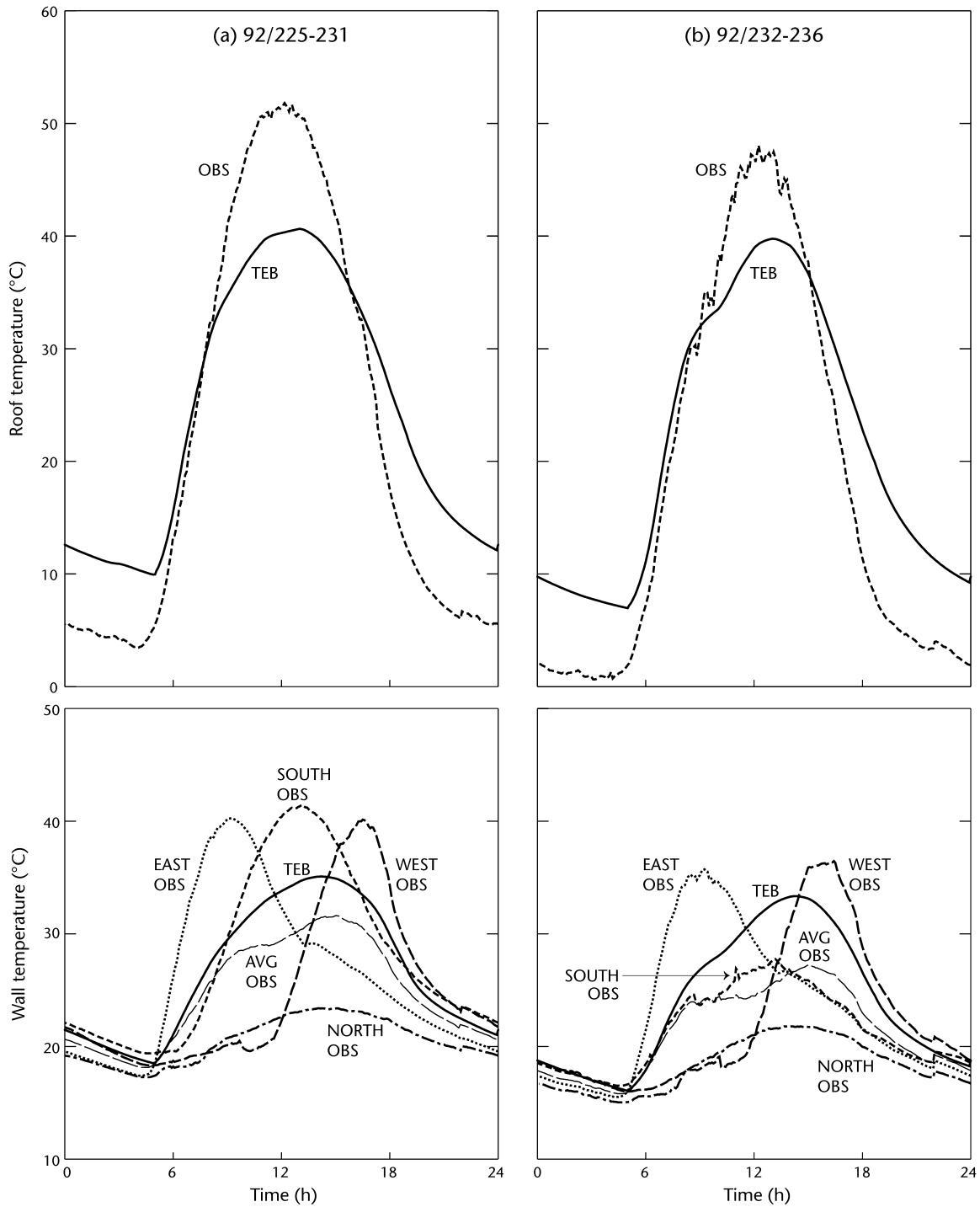


FIG. 6. Ensemble mean diurnal cycle of observed (microscale) and modeled (TEB) surface temperature for the Vancouver site for (a) YD 225–231 and (b) YD 232–236: (top) roof and (bottom) individual N-, E-, S-, and W-facing walls and average, and simulated wall temperature.

6). TEB simulates a smaller amplitude than is observed (the reverse of the Me93 case). TEB does reproduce the general form of the nocturnal cooling pattern, but observed roof temperatures are low at night and the model overestimates them by 8 K, on average. The roof where

the surface temperature observations were conducted is unrepresentative of the local scale (see section 4), thus the poor comparisons are not unexpected. TEB is in somewhat better agreement with the airborne roof data of the morning and evening flights but underestimates

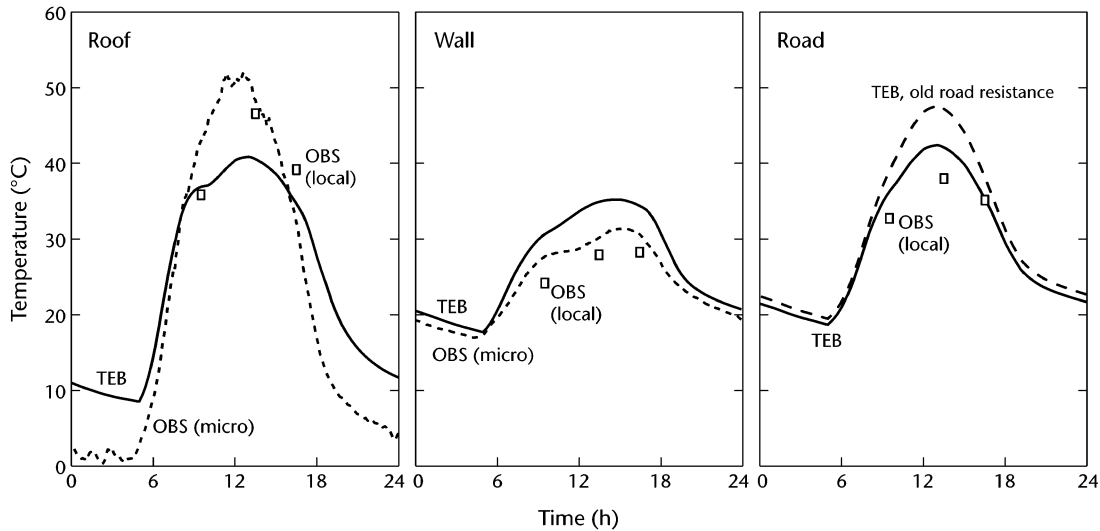


FIG. 7. Time series of observed (micro- and local scale) and modeled (TEB) surface temperatures for YD 228: (left) roof, (middle) averaged microscale and local-scale wall temperature, and (right) local-scale road temperature. Simulated road surface temperature: Masson (2000) scheme [road resistance follows Rowley et al. (1930)] and new roughness length formulation.

the early afternoon value, which is near the daily maximum, by approximately 6 K (Fig. 7).

The TEB wall temperature is evaluated against the average of the observed wall temperatures (north, east, south, and west facing). For sunny days in period 1, TEB wall temperatures are similar to this averaged wall temperature (Table 3). The bias and root-mean-square error (rmse) between TEB and the observations are small (1.9 and 2.4 K, respectively). Note that the difference is slightly larger when compared to the airborne measurements; the overestimation probably reaches 5 K in the daytime (Fig. 7), but the maximum wall temperature near 1600 LST is reproduced. However, a discrepancy appears for period 2. On the sunny days of period 1, the individual wall temperatures follow a standard daytime pattern and the mean wall temperature peaks at about 1600 LST (Fig. 6a). In period 2, on the other hand, there is significant cloud cover in the middle of the day. While three of the walls show little change from period 1, the temperature of the south-facing wall was considerably cooler (Fig. 6b). TEB does not capture the magnitude of this reduced warming (except for the cloudiest day, not shown) and model performance is correspondingly poorer. It seems the temporal history of warming of the individual walls over the day, and its disruption by cloud, is responsible. Such temporal specificity is not incorporated in the generic wall approach of TEB. If this is correct, this type of impact can be expected to be greatest in cases of urban geometry with low building height-to-street width ratios, as is the case at the V192 site.

Overall, however, the good agreement between the wall temperature measurement and TEB output, especially when radiative forcing is symmetric through the day, supports one of the main simplifications of the

scheme: the use of only one wall temperature that is independent of orientation.

For roads, the airborne-based measurements can be stratified into shaded and sunlit fractions. The sunlit fraction is much larger, because of the small height of the buildings (Voogt and Grimmond 2000). The road temperature, averaged according to sunlit and shaded areas, reaches 38°C in the afternoon of YD 228. TEB simulates only one road temperature, which is comparable to the local-scale observation. TEB simulates it well, with an overestimation of only 3–4 K at midday (Fig. 7). The simplification of TEB to consider only one road temperature is also supported by this comparison.

To illustrate the improvement resulting from the new parameterizations (see section 4), TEB was run with the old formulation of the road aerodynamic resistance (Fig. 7). The main problem with the original TEB predictions is an increase of the temperature during the day, 6 K higher than with the new version. The new roughness length formulation creates a larger conductance, and thus a larger Q_H , leading to better agreement between the modeled temperature and the observations. Since the road surface at the V192 site is large, and has an important role for the exchanges from the canyons (walls are low), this validation is particularly pertinent.

2) ENERGY FLUXES AT THE LOCAL SCALE

TEB correctly reproduces Q^* during the entire period (Fig. 8). As Table 5 shows this is true for the overall set (bias = -9 W m^{-2}) and for both day and night (biases of -17 and $+2 \text{ W m}^{-2}$, respectively).

When comparing modeled and measured data it is important to consider the potential for measurement errors and uncertainties. Here, the observed fluxes and

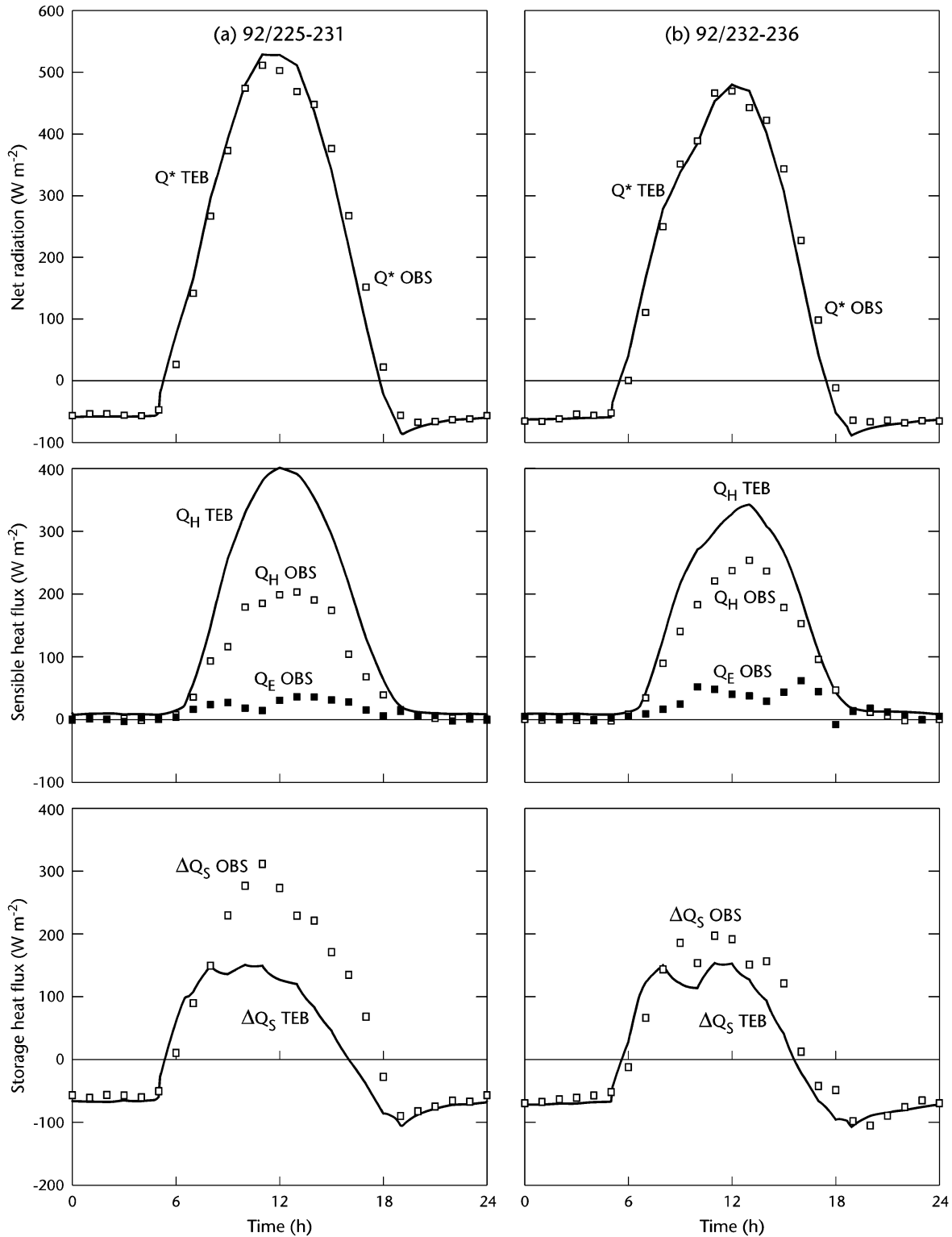


FIG. 8. Ensemble mean diurnal cycle of measured and modeled surface energy balance fluxes for the Vancouver site, for (a) YD 225–231 and (b) YD 232–236: (top) net radiation, (middle) total turbulent heat flux, and (bottom) storage sensible heat flux.

TABLE 5. Performance statistics for TEB for heat fluxes at the Vancouver light industrial site (as in Table 4).

		Days 223–236			Days 225–231			Days 232–236		
		Q^*	$Q_H + Q_E$	ΔQ_S	Q^*	$Q_H + Q_E$	ΔQ_S	Q^*	$Q_H + Q_E$	ΔQ_S
Overall period	Obs	150	95	55	161	87	74	136	103	32
	TEB	141	133	8	159	147	12	126	119	6
	Bias	-9	38	-47	-2	60	-62	-10	16	-26
	Rmse	59	76	91	57	97	105	59	50	66
Daytime	Obs	323	168	156	318	143	175	323	196	126
	TEB	306	234	73	313	243	70	301	225	76
	Bias	-17	66	-83	-5	100	-105	-21	29	-50
	Rmse	76	103	121	72	127	136	77	69	89
Nighttime	Obs	-59	7	-66	-62	7	-69	-56	8	-64
	TEB	-57	11	-68	-59	11	-70	-55	11	-66
	Bias	2	4	-2	3	4	-1	1	3	-2
	Rmse	24	12	23	20	11	19	27	13	26

meteorological conditions at the V192 site were compared with concurrent observations made at a residential site (sunset, Vs92; Grimmond and Oke 1999b). In urban areas, Q^* is expected to be fairly conservative spatially (Schmid et al. 1991; Oke 1997). Comparison of the data collected concurrently at the two Vancouver sites shows only small differences in Q^* ; the largest differences $< 50 \text{ W m}^{-2}$ occur in the late morning when Q^* at V192 is larger. This indicates reason for confidence in the V192 Q^* data.

During night, the measurements show relatively large ΔQ_S , with a peak release just after sunset. This allows a positive Q_H to be maintained during the first hours of the night. Then ΔQ_S equilibrates close to the value of Q^* , and Q_H is small for the rest of the night. In terms of the observed storage heat flux, it is important to recall that it is computed here as the residual of the measured energy balance and thus errors in any of the other fluxes accumulate in ΔQ_S . However, during night, fluxes other than Q^* and ΔQ_S are small (see the measured Q_H and Q_E) or negligible (Q_F or ΔQ_A). The warehouses in the V192 area have minimal heating or air conditioning, few chimneys, and traffic is light in the day and negligible at night. The ΔQ_A is negligible, because nocturnal winds are weak except on one night. Therefore,

the observed nocturnal ΔQ_S is probably reliable. TEB simulates this nocturnal storage pattern well (bias = -2 W m^{-2} , rmse $< 23 \text{ W m}^{-2}$ throughout the period; see Table 5). The net energy storage of the model during YD 226–231 is 0.4 MJ m^{-2} , corresponding to a mean storage heat flux of about $+0.8 \text{ W m}^{-2}$, or a 3 K heating of a 0.1-m layer of soil or concrete. This buildup of heat is consistent with results from heat flux plates installed at the site (not shown). Note that hourly values are not necessarily good, but the modeled integrated daily heat uptake is about right.

During the day, observed Q_H is large and Q_E is small. In the drought conditions of the measurement period, TEB partitions Q^* between ΔQ_S and Q_H . For period 2 (Fig. 8b) and YD 224, 225 (not shown), there is reasonable correspondence between the predictions of TEB and the measured sensible heat fluxes (Table 5). The hysteresis behavior of ΔQ_S (Fig. 9) is slightly overestimated. For period 1, however, TEB significantly overpredicts Q_H , while measurements show a much larger ΔQ_S than TEB (Fig. 8a). This discrepancy may be due to an overestimation of observed ΔQ_S [in (2)], through the neglect of ΔQ_A . During period 1, the wind direction is predominantly from the west so there may be a sea breeze (Oke and Hay 1994). Under these circumstances it is possible that the lack of ability to evaluate the advection term in both the measurements and the model results prevents a more appropriate comparison of the fluxes. As noted in section 2, the advection flux in the box ΔQ_A appears in the Q_H term at the top of the box when modeled offline and in the ΔQ_S term in the observations. An improved estimate would come from running the model in the 3D mode.

6. Sensitivity of the scheme

The ability of the TEB scheme to reproduce most features of surface–atmosphere energy exchanges and the resultant surface temperatures of relatively dry urban districts has been demonstrated. However, many model input properties and some of the forcing data (e.g., radiation) are subject to uncertainties. Therefore, the sen-

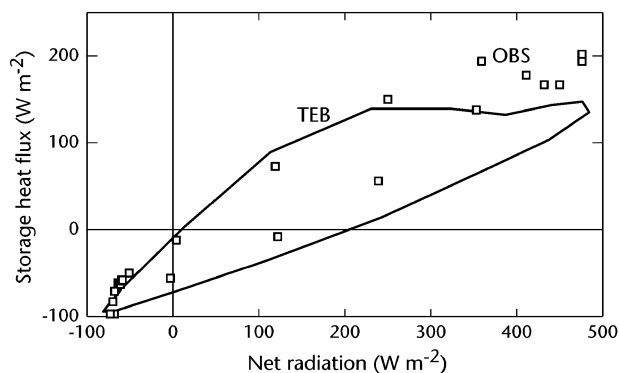


FIG. 9. Ensemble mean measured and modeled (TEB) hysteresis loop relating the storage heat flux to the net radiation at the Vancouver light industrial site for YD 232–236.

TABLE 6. Sensitivity analysis to varying TEB input parameters relative to the reference case for Mexico City.

	Max Q^* ($W m^{-2}$)	Daytime $\Delta Q_s/Q^*$	Nocturnal Q^* ($W m^{-2}$)	Nocturnal Q_H ($W m^{-2}$)	T_{roof} bias (K)	T_{wall} bias (K)	T_{road} bias (K)
Reference	439	0.56	-82	+14			
Geometric parameters							
Building fraction + 0.10 ($\rightarrow H/W = 1.42$)	+1	-0.01	+1				+0.1
Building fraction - 0.10 ($\rightarrow H/W = 1.03$)	+1	+0.01	-1				-0.1
Wall/plane area ratio + 0.20 ($\rightarrow H/W = 1.40$)	+6	+0.01	-2	+3			+0.1
Wall/plane area ratio - 0.20 ($\rightarrow H/W = 0.96$)	-3	-0.01	+2	-3		-0.1	-0.1 ($\sigma = 0.7$)
Radiative parameters							
Roof albedo + 0.10	-32	+0.03	+2	-1	-1.3 ($\sigma = 1$)		
Wall albedo + 0.10	-6			-1		-0.4	+0.1
Road albedo + 0.10	-6						-0.4
Roof emissivity - 0.05	+4	-0.01	+1	+1	+0.5		
Wall emissivity - 0.05						-0.2	
Road emissivity - 0.05						-0.1	+0.1
Thermal parameters							
Roof thickness $\times 2$	-8	-0.04	+4	-2	-0.4 ($\sigma = 2.2$)		
Wall thickness \div by 2				-1		-0.1	
Road thickness \div by 2	+2	+0.01	-1	+1			+0.2 ($\sigma = 1.2$)
Roughness lengths							
Town $z_0 \div$ by 2	-2	+0.02	-1			+0.4	+0.5
Town $z_0 \times 2$	+3	-0.02	+1			-0.6	-0.6
Road $z_0 \div$ by 5	-1	+0.01		-2			+0.5
Road $z_0 \div$ by 5	-11	+0.05	-2	+1	+1.5 ($\sigma = 1.2$)		
Temperature initialization							
Internal building temperature + 5 K	-1	-0.01	-1	+1	+0.2	+0.1	+0.1
Road and deep soil temperature + 5 K	-1	-0.01	-1	+2		+0.2	+0.6
Forcing							
Incoming infrared - 20 $W m^{-2}$	-12	+0.04	-10	-5	-1.9	-0.7	-1.1
Incoming solar - 10%	-49	+0.03	+2	-3	-1.1 ($\sigma = 0.8$)	-0.6	-0.7
Modification of resistance							
Without new road resistance							+0.1

sitivity of the scheme to input parameters was tested via dedicated runs across a wide range of values for each parameter. Tables 6 and 7 list the modifications and the resulting sensitivity of the calculated fluxes and temperatures. Comparisons are made against a reference run.

Daytime Q^* is relatively insensitive to most parameters except for the albedo of horizontal surfaces, the roof roughness length, and $K\downarrow$. Geometric parameters modify Q^* to a lesser extent (canyon aspect ratios vary in the range ± 0.2 from the reference). The effect of roofs is always the most important, because there is no trapping effect for this surface. Because of the geometry of the site, the road albedo has a very small impact for Me93. Nighttime Q^* also is not very sensitive, except to the calculated $L\downarrow$, the roof thickness or its thermal structure (for V192), and the building fraction, if the

road and roof energy balances are very different (as is the case in V192).

The $\Delta Q_s/Q^*$ ratios for these sensitivity analyses, are in the range 0.26–0.31 and 0.52–0.61 for V192 and Me93, respectively. For most parameters, variations in input values result in differences of less than 2% in $\Delta Q_s/Q^*$ between runs. Because only dry sites are involved this also means the scheme is stable with respect to the partitioning between the storage and turbulent sensible heat fluxes. For the V192 simulation, $\Delta Q_s/Q^*$ is sensitive to roof roughness length (because it is a major control on the convective/conductive sensible heat sharing between the air and the roof). A large impact is found for the choice of the road aerodynamic resistance. The road surface temperature measurements at V192 enabled us to discriminate between the two formulations (see section 5b). A too-small roughness length for roads

TABLE 7. Sensitivity analysis to varying TEB input parameters relative to the reference case for Vancouver.

	Max Q^* (W m ⁻²)	Daytime $\Delta Q_s/Q^*$	Nocturnal Q^* (W m ⁻²)	Nocturnal Q_H (W m ⁻²)	T_{roof} bias (K)	T_{wall} bias (K)	T_{road} bias (K)
Reference	520	0.28	-61	14			
Geometric parameters							
Building fraction + 0.10 ($\rightarrow H/W = 0.50$)	-5	-0.02	+4	-2		-0.1	-0.3
Building fraction - 0.10 ($\rightarrow H/W = 0.33$)	+3	+0.02	-4	+1			+0.1
Wall/plane area ratio + 0.20 ($\rightarrow H/W = 0.60$)	+1	+0.02	-1	+2	+0.1		-0.4
Wall/plane area ratio - 0.20 ($\rightarrow H/W = 0.19$)	-3	-0.02	+2	-2	-0.1		+0.4
Radiative parameters							
Roof albedo + 0.10	-34	+0.01			-1.0 ($\sigma = 0.9$)		
Wall albedo + 0.10	-4			-1		-0.6	
Road albedo + 0.10	-21		+1	-1		-0.2	-0.8
Roof emissivity - 0.05	+4				+0.3		
Wall emissivity - 0.05						+0.1	
Road emissivity - 0.05	+2		+1	+1			+0.2
Thermal parameters							
Roof thickness $\times 2$	+2	+0.02	-6	+3	+0.8 ($\sigma = 2.3$)		
Wall thickness \div by 2			+1	-2		-0.3	-0.1
Road thickness \div by 2	+2	+0.01	-2	+4		+0.1	+0.2
Steel roof (see text)	-2	-0.02	+5	-1	-0.7 ($\sigma = 2.2$)		
Roughness lengths							
Town $z_0 \div$ by 2	-3	+0.01	-1	+1		+0.6	+0.6
Town $z_0 \times 2$	+3	-0.01	+1	+1		-0.6	-0.6
Road $z_0 \div$ by 5	-8	+0.02	-2				+1.9 ($\sigma = 1.0$)
Roof $z_0 \div$ by 5	-18	+0.03	-1		+1.9 ($\sigma = 2.0$)		
Temperature initialization							
Building internal temperature + 5 K	-1	-0.01	-1	+1	+0.1	+0.1	+0.1
Surface and deep soil temperature + 5 K			-1			+0.1	+0.3
Forcing							
Incoming infrared - 20 W m ⁻²	-15	+0.02	-9	-4	-1.6 ($\sigma = 0.9$)	-0.9	-1.0
Incoming solar - 10%	-58	+0.01	+2	-2	-0.8 ($\sigma = 0.7$)	-0.9	-1.0
Air temperature - 2 K	+10	-0.02	+4	+4	-0.9	-1.2	-1.3
Modification of resistance							
Without building room resistances	+2	+0.03	+3	-3	-0.5	-1.0	-0.3
Without new road resistance	-9	+0.02	-2	+3			+1.8 ($\sigma = 1.4$)

leads to an overestimate of the surface temperature during daytime (by 10 K, not shown), which in turn leads to too-large heat storage (Table 7). The impact of modifying the internal building resistance is significant, and it improves the roof temperature, especially at night (not shown). Some warehouses in the V192 study area have roofs made of gravel on steel, instead of gravel on steel and wood. Using such a roof in TEB (20 mm gravel, 0.50 mm steel, 10 mm wood) decreases the storage and gives a $\Delta Q_s/Q^*$ ratio of 0.26. This dampens the thermal response of the roof surface (especially at night) compared to microscale measurements on this type of roof (not shown). This signals the need to take care in setting the value of the roof parameters for such cases. For the Me93 site, the roof specification again has a large impact, as does the radiative forcing.

The road and wall temperatures simulated by TEB are not much affected by uncertainties in the radiative and thermal input parameters. In contrast, the roof temperature is sensitive, both on average (bias) and its diurnal evolution (standard deviation), particularly to the

albedo assigned. All temperatures are sensitive to incoming radiation and the roughness length.

Summarizing the results of the sensitivity tests it seems that emissivities, temperature initializations, and wall characteristics have little impact. Similarly, the output is relatively insensitive to the overall roughness length for the city, even when large variations were considered. Road characteristics are not critical, except perhaps for albedo in areas with low buildings and wide roads. Errors in assigning geometric parameters have a moderate impact. Uncertainties in setting incoming radiative fluxes are significant. Thus we recommend that, if possible, measured values be used. Care must be taken not to use roughness values for horizontal surfaces that are too small and to take careful note of roof characteristics. However, it is our view that for the conditions tested, TEB is robust. To put this in perspective, across the range of sensitivity conditions tested here, the $\Delta Q_s/Q^*$ ratio is always within 5% of the reference run.

7. Concluding comments

Evaluation of TEB using field observations from two relatively dry and sparsely vegetated urban areas, with very different urban structure, suggests that overall the model performs well. The evaluation process resulted in small modifications to the original TEB scheme; these were in the aerodynamic resistance formulations. The agreement between the measurements and TEB gives some support to one of the simplifications of the scheme: the use of only one wall temperature.

The results of this evaluation are informative not only in assessing the ability of the model to calculate fluxes and thermal responses in these urban settings, but also in aiding interpretation of existing field data and to inform the better design of future observational programs. For example, the effect of the timing of clouds in sites with different canyon geometries, and the role of advection both in measurements and modeling need further investigation. Next we intend to extend the evaluation to include vegetated and moist urban districts using the combined TEB-ISBA scheme.

This study is perhaps the first to attempt genuine validation of the output of an urban land surface model that is designed for use within a mesoscale atmospheric model. Several previous studies have provided comparisons with field data from standard climate stations, especially with regard to air temperature, but none has checked output against observed fluxes and temperatures together. Agreement against air temperature can be relatively easily achieved, but when agreement is between fluxes and surface temperatures, it shows that the energetic processes underlying the thermal estimates are also physically realistic.

Significant difficulties remain with obtaining high quality measurements of surface fluxes. Energy balance closure is not achieved even in simple rural sites. In the urban case, uncertainties associated with anthropogenic releases of heat, water, and pollutants including radiatively active aerosols and gases from concentrated and sometimes organized source distributions, and microadvection that characterizes exchanges in among elements of the urban canopy layer contribute to uncertainty in fluxes, especially heat storage change, if it is resolved as a residual. Nevertheless, the estimates from several cities show similar features; this gives some confidence that anomalous effects do not dominate in the balance.

Similarly, there are challenges for modeling. Not least is the need to strike a balance between the detail and complexity of the modeled phenomena on the one hand and the simplicity of input properties and computational efficiency on the other. Given certain conceptual and practical difficulties we also note the difficulty of getting model output and observations to apply to a common "surface" or atmospheric plane.

The TEB model and the nature of the observational database used in the present study were not designed together. One of the issues that this research draws at-

tention to is the importance of scale and ensuring that the measurement and modeling communities are both cognizant of this. Better and more comprehensive observational data will emerge and both our understanding of the physics of the urban atmosphere and computational capacity will grow, but in our judgment the present comparison of observed and modeled climatic conditions represents a reasonable convergence of present-day capabilities of measurement and simulation.

Acknowledgments. This work has been supported by grants to the authors by the Centre National de Recherches Météorologiques, the Centre National de Recherches Scientifiques de France, the National Science Foundation, the Natural Sciences and Engineering Research Council of Canada, and the Canadian Foundation for Climate and Atmospheric Science. The authors are very grateful to the following colleagues who supplied data or provided assistance with interpretations: Stephanie Meyn of the University of British Columbia; Dr. Rachel Spronken-Smith of the University of Canterbury; Dr. Agustín Muhlia Velázquez, Coordinador del Observatorio de Radiación Solar, Instituto de Geofísica, UNAM; and Dr. James Voogt of the University of Western Ontario.

REFERENCES

- Arnfield, A. J., and C. S. B. Grimmond, 1998: An urban canyon energy balance model and its application to urban storage heat flux modelling. *Energy Build.*, **27**, 61–68.
- , J. M. Herbert, and G. T. Johnson, 1998: A numerical simulation investigation of urban canyon energy budget variations. Preprints, *Second Symp. on the Urban Environment*, Albuquerque, NM, Amer. Meteor. Soc., 2–5.
- ASHRAE, 1989: *ASHRAE Handbook: 1989 Fundamentals*. ASHRAE, 37 sections + errata + index, 797 pp.
- Best, M., 1998: Representing urban areas in numerical weather prediction models. Preprints, *Second Symp. on the Urban Environment*, Albuquerque, NM, Amer. Meteor. Soc., 148–151.
- Foken, T., and S. Oncley, 1995: Results of the workshop "Instrumental and Methodical Problems of Land Surface Flux Measurements." *Bull. Amer. Meteor. Soc.*, **76**, 1191–1193.
- Grimmond, C. S. B., and T. R. Oke, 1999a: Aerodynamic properties of urban areas derived from analysis of surface form. *J. Appl. Meteor.*, **38**, 1262–1292.
- , and —, 1999b: Heat storage in urban areas: Local-scale observations and evaluation of a simple model. *J. Appl. Meteor.*, **38**, 922–940.
- , and —, 2002: Turbulent heat fluxes in urban areas: Observations and local-scale urban meteorological parameterization scheme (LUMPS). *J. Appl. Meteor.*, **41**, 792–810.
- Ichinose, T., K. Shimodozono, and K. Hanaki, 1999: Impact of anthropogenic heat on urban climate in Tokyo. *Atmos. Environ.*, **33**, 3897–3909.
- Lafore, J., and Coauthors, 1998: The Meso-NH atmospheric simulation system. Part I: Adiabatic formulation and control simulation. *Ann. Geophys.*, **16**, 90–109.
- Lee, X., 1998: On micrometeorological observations of surface-air exchange over tall vegetation. *Agric. Forest Meteorol.*, **91**, 39–49.
- Masson, V., 2000: A physically-based scheme for the urban energy balance in atmospheric models. *Bound.-Layer Meteorol.*, **94**, 357–397.

- McMullan, R., 1992: *Environmental Science in Building*. 3d ed. Macmillan, 332 pp.
- Mills, G., 1997: An urban canopy-layer climate model. *Theor. Appl. Climatol.*, **57**, 229–244.
- Noilhan, J., and S. Planton, 1989: A simple parameterization of land surface processes for meteorological models. *Mon. Wea. Rev.*, **117**, 536–549.
- Oke, T. R., 1987: *Boundary Layer Climates*. 2d ed. Routledge, 435 pp.
- , 1988: The urban energy balance. *Prog. Phys. Geogr.*, **12**, 471–508.
- , 1997: Urban environments. *The Surface Climates of Canada*, W. G. Bailey, T. R. Oke, and W. R. Rouse, Eds., McGill–Queen's University Press, 303–327.
- , and J. E. Hay, 1994: *The Climate of Vancouver*. B.C. Geographical Series, No. 50, 84 pp.
- , R. A. Spronken-Smith, E. Jauregui, and C. S. B. Grimmond, 1999: The energy balance of central Mexico City during the dry season. *Atmos. Environ.*, **33**, 3919–3930.
- Prata, A. J., 1996: A new long-wave formula for estimating downward clear-sky radiation at the surface. *Quart. J. Roy. Meteor. Soc.*, **122**, 1127–1151.
- Rotach, M. W., 1995: Profiles of turbulence statistics in and above an urban street canyon. *Atmos. Environ.*, **29**, 1473–1486.
- Rowley, F. B., A. B. Algren, and J. L. Blackshaw, 1930: Surface conductances as affected by air velocity, temperature and character of surface. *ASHRAE Trans.*, **36**, 429–446.
- Schmid, H. P., H. A. Cleugh, C. S. B. Grimmond, and T. R. Oke, 1991: Spatial variability of energy fluxes in suburban terrain. *Bound.-Layer Meteor.*, **54**, 249–276.
- Taha, H., 1999: Modifying a mesoscale meteorological model to better incorporate urban heat storage: A bulk parameterization approach. *J. Appl. Meteor.*, **38**, 466–473.
- Voogt, J. A., and T. R. Oke, 1997: Complete urban surface temperatures. *J. Appl. Meteor.*, **36**, 1117–1132.
- , and C. S. B. Grimmond, 2000: Modeling surface sensible heat flux using surface radiative temperatures in a simple urban area. *J. Appl. Meteor.*, **39**, 1679–1699.